(the approximate midpoint of the scaling regime; movie S2). Differences in spindle lengths for these two extract droplet geometries were statistically indistinguishable (Student's t test, $P = 0.2$ for all slug and sphere data between 40 and 60 μm). Furthermore, spindle length remained relatively constant despite threefold increases in slug length over a narrow range of cytoplasmic volumes (Fig. 3, B and C, and fig. S3). Collectively, these results oppose the predictions of a boundary-sensing model for spindle length regulation and suggest that cytoplasmic shape is not likely a major determinant of spindle length.

Through a variety of different mechanisms, spindles in vivo demonstrate a remarkable ability to correctly position themselves near the cell center before the onset of anaphase and cytokinesis. (*16*–*20*). Each implicitly requires the spindle be able to "sense" its position relative to cellular boundaries. In the absence of boundary sensing, spindle position within a cell (or a confining extract volume) is expected to be random. To test this prediction, we plotted spindle position relative to the volumetric centers of confining spheres and slugs (Fig. 4, A and B). In both geometries, spindles tended to localize toward the droplet center to a greater extent than expected for uniform random positioning (Fig. 4, A and B, and movie S3). This trend was more pronounced in smaller droplets (Fig. 4, A and B, residual plots). In contrast, the positions of encapsulated polystyrene beads aligned more closely with average random positions (Fig. 4, A and B, residual plots; figs. S1 and S2; and movie S4). This suggested that the weak convective flows observed in some slugs were likely not responsible for spindle centering (e.g., movie S5). The distribution of spindle orientations relative to the slug long axis was found to be 31° ± 16° (Fig. 4C), indicating that, like in cells, a spindle is more likely to align parallel to the long axis of its enclosure (*21*), even in the absence of a cortical membrane and associated pulling forces. Indeed, peripheral spindle microtubules extend well beyond the spindle proper, effectively increasing its size (*22*). Perhaps these peripheral microtubules exert pushing forces against droplet boundaries that result in centering (*23*). Alternatively, spindle proximity to a droplet boundary might influence the distribution of forces generated by microtubule-associated motors pulling against the bulk cytoplasm (*19*, *24*). Thus, a boundary-sensing mechanism might indeed work to affect spindle position but contributes little, if at all, to determining spindle length.

Collectively, our data indicate that changes in cytoplasmic volume are sufficient to account for spindle scaling as it occurs in vivo (*2*). By eliminating alternative hypothetical models, the data support a scaling mechanism in which a limiting pool of cytoplasmic component(s) regulates spindle length (*8*, *11*). In large droplets or cells, like in unbounded extract, spindle length appears to be constrained by mechanisms intrinsic to the spindle (*2*, *25*). Once cytoplasmic volume is reduced to a critical threshold, components become limited, which produces smaller spindles. This process serves as a passive yet robust way for cells to control the size of their spindles and possibly other internal structures.

References and Notes

1. M. Montorzi, M. H. Burgos, K. H. Falchuk, *Mol. Reprod. Dev.* **55**, 75–82 (2000).
2. M. Wühr *et al.*, *Curr. Biol.* **18**, 1256–1261 (2008).
3. A. Courtois, M. Schuh, J. Ellenberg, T. Hiiragi, *J. Cell Biol.* **198**, 357–370 (2012).
4. Y. Hara, A. Kimura, *Curr. Biol.* **19**, 1549–1554 (2009).
5. S. L. Bird, R. Heald, K. Weis, *Mol. Biol. Cell* **24**, 2506–2514 (2013).
6. T. Kiyomitsu, I. M. Cheeseman, *Nat. Cell Biol.* **14**, 311–317 (2012).
7. D. J. Sharp *et al.*, *Mol. Biol. Cell* **11**, 241–253 (2000).
8. M. Decker *et al.*, *Curr. Biol.* **21**, 1259–1267 (2011).
9. W. B. Ludington, L. Z. Shi, Q. Zhu, M. W. Berns, W. F. Marshall, *Curr. Biol.* **22**, 2173–2179 (2012).
10. Y. H. Chan, W. F. Marshall, *Organogenesis* **6**, 88–96 (2010).
11. N. W. Goehring, A. A. Hyman, *Curr. Biol.* **22**, R330–R339 (2012).
12. A. Desai, A. W. Murray, T. Mitchison, C. E. Walczak, in *Mitosis and Meiosis*, C. L. Rieder, vol. 61 of *Methods in Cell Biology* (Academic Press, New York, 1999), pp. 385–412.
13. J. Newport, M. Kirschner, *Cell* **30**, 675–686 (1982).
14. P. D. Nieuwkoop, J. Faber, Eds., *Normal Table of* Xenopus laevis *[Daudin] - A Systematical and Chronological Survey of the Development from the Fertilized Egg Till the End of Metamorphosis* (North-Holland, Amsterdam, ed. 2, 1967).
15. J. D. Wilbur, R. Heald, *Elife* **2**, e00290 (2013).
16. P. Gönczy, S. Grill, E. H. Stelzer, M. Kirkham, A. A. Hyman, in *The Cell Cyle and Development*, G. R. Bock, G. Cardew, J. A. Goode, Eds. (Novartis Foundation Symposium no. 237, Wiley, Chichester, UK, 2008), pp. 164–181.
17. L. Lee *et al.*, *Science* **287**, 2260–2262 (2000).
18. N. Minc, D. Burgess, F. Chang, *Cell* **144**, 414–426 (2011).
19. T. Mitchison *et al.*, *Cytoskeleton* **69**, 738–750 (2012).
20. I. M. Tolić-Nørrelykke, L. Sacconi, G. Thon, F. S. Pavone, *Curr. Biol.* **14**, 1181–1186 (2004).
21. M. Wühr, E. S. Tan, S. K. Parker, H. W. Detrich 3rd, T. J. Mitchison, *Curr. Biol.* **20**, 2040–2045 (2010).
22. J. C. Gatlin *et al.*, *Curr. Biol.* **19**, 287–296 (2009).
23. T. E. Holy, M. Dogterom, B. Yurke, S. Leibler, *Proc. Natl. Acad. Sci. U.S.A.* **94**, 6228–6231 (1997).
24. M. Wühr, S. Dumont, A. C. Groen, D. J. Needleman, T. J. Mitchison, *Cell Cycle* **8**, 1115–1121 (2009).
25. S. Dumont, T. J. Mitchison, *Curr. Biol.* **19**, R749–R761 (2009).

Acknowledgments: We thank T. Salmon and T. Mitchison for their insightful reviews of the manuscript; M. Wuhr for comments on the work and for providing access to raw data originally presented in (*2*); L. Edens, C. Geisler, D. Fay, and D. Levy in the Molecular Biology Department at the University of Wyoming for their critical review of the manuscript and helpful suggestions; and A. Groen for providing labeled anti-NuMA used in these studies. This work was supported by NIH grants R01 GM102428 (to J.C.G.) and R15 GM101636 (to J.O.) and by the NIH-funded Wyoming IDeA Networks of Biomedical Research Excellence program (P20RR016474 and P20GM103432).

Supplementary Materials

www.sciencemag.org/content/342/6160/853/suppl/DC1
Materials and Methods
Supplementary Text
Figs. S1 to S3
References (*26*–*31*)
Movies S1 to S5

12 July 2013; accepted 15 October 2013
10.1126/science.1243110

Cytoplasmic Volume Modulates Spindle Size During Embryogenesis

Matthew C. Good,[1,2,3] Michael D. Vahey,[2] Arunan Skandarajah,[2] Daniel A. Fletcher,[2,4]* Rebecca Heald[1]*

Rapid and reductive cell divisions during embryogenesis require that intracellular structures adapt to a wide range of cell sizes. The mitotic spindle presents a central example of this flexibility, scaling with the dimensions of the cell to mediate accurate chromosome segregation. To determine whether spindle size regulation is achieved through a developmental program or is intrinsically specified by cell size or shape, we developed a system to encapsulate cytoplasm from *Xenopus* eggs and embryos inside cell-like compartments of defined sizes. Spindle size was observed to shrink with decreasing compartment size, similar to what occurs during early embryogenesis, and this scaling trend depended on compartment volume rather than shape. Thus, the amount of cytoplasmic material provides a mechanism for regulating the size of intracellular structures.

Although mechanisms that set eukaryotic cell size by coordinating growth and division rates have been uncovered (*1*–*3*), much less is known about how the size and the shape of a cell affect its physiology. Recent work has suggested mechanisms by which cell boundaries or size can control biochemical reactions (*2*), constrain cytoskeletal assembly (*4*–*6*), and dictate the positioning of internal structures (*7*, *8*). The size-scaling problem is most acute during early embryo development, when cell size changes rapidly. For example, over the first 10 hours of amphibian embryogenesis, cell diameter may decrease 100-fold, from a 1.2-mm egg to 12-μm-diameter blastomeres, because of cell division in

[1]Department of Molecular and Cellular Biology, University of California–Berkeley, Berkeley, CA 94720, USA. [2]Department of Bioengineering and Biophysics Group, University of California–Berkeley, Berkeley, CA 94720, USA. [3]Miller Institute for Basic Research in Science, University of California–Berkeley, Berkeley, CA 94720, USA. [4]Physical Biosciences Division, Lawrence Berkeley National Laboratory, Berkeley, CA 94720, USA.

*Corresponding author. E-mail: bheald@berkeley.edu (R.H.), fletch@berkeley.edu (D.A.F.)

the absence of growth (*9*). Although micrometer-scale organelles and intracellular structures have been shown to adapt and function across a wide spectrum of cell sizes (*10*–*14*), mechanisms of size scaling remain poorly understood.

We focused on the mitotic spindle, a dynamic bipolar structure consisting of microtubules and many associated factors that must be appropriately sized to accurately distribute chromosomes to daughter cells. During development, spindle size correlates with cell size in the embryos of invertebrates (*15*, *16*), amphibians (*9*) (fig. S1), and mammals (*17*). However, it is unknown whether spindle size is governed by compositional changes as part of a developmental blueprint or whether spindle size is coupled directly to physical properties of the cell, such as size and shape. Although molecular mechanisms of spindle size regulation have been proposed (*9*–*13*), the existence of a causal link between cell size and spindle size remains unclear.

Because of the difficulty of modulating cell size in vivo, we investigated spindle size scaling by developing an in vitro system of cell-like droplets of varying size containing *Xenopus* egg or embryo cytoplasm. *Xenopus* egg extracts transit the cell cycle in the absence of cell boundaries and recapitulate many cell biological activities in vitro, including spindle assembly (*18*, *19*). To match cell size changes during *Xenopus* embryogenesis, we tuned compartment volume 1,000,000-fold by using microfluidic systems (Fig. 1A and fig. S2). A polyethylene glycol (PEG)–ylated stearate served as a surfactant to prevent droplets from coalescing and to prevent cytoplasmic proteins from interacting with the boundary (Fig. 1A).

Metaphase spindle length and width scaled with droplet size in vitro (Fig. 1, B and C, and fig. S3). Spindles, which normally have a steady-state length of 35 to 40 μm in bulk egg extract (*20*), became smaller as the size of the encapsulating droplet decreased (Fig. 1C and fig. S3). Spindle size scaling was roughly linear in droplet diameters ranging from 20 to 80 μm (Fig. 1C), whereas in larger droplets spindle size matched that of unencapsulated egg extracts. Spindle assembly efficiency decreased in very small droplets and dropped to zero in droplets with a diameter less than 20 μm (fig. S3, C and D). Thus, two regimes of scaling were observed: one in which spindle size was coupled to droplet diameter and a second in which they were uncoupled. These two regimes were similar to spindle scaling trends observed in vivo during early *Xenopus* embryogenesis (Fig. 1, C and D, and fig. S1B) (*9*). Thus, compartmentalization is sufficient to recapitulate spindle size scaling during embryogenesis in the absence of any developmental cues (e.g., transcription).

We considered two possible explanations for the scaling of spindle size with cell or droplet size. The position of cell or droplet boundaries could directly influence spindle size through interaction with microtubules. Alternatively, cytoplasmic volume could limit the amount of material for assembly, which has been proposed for centrosome size regulation in *Caenorhabditis elegans* (*12*, *21*) and spindle size regulation in mouse and sea snail embryos (*17*, *22*). To distinguish

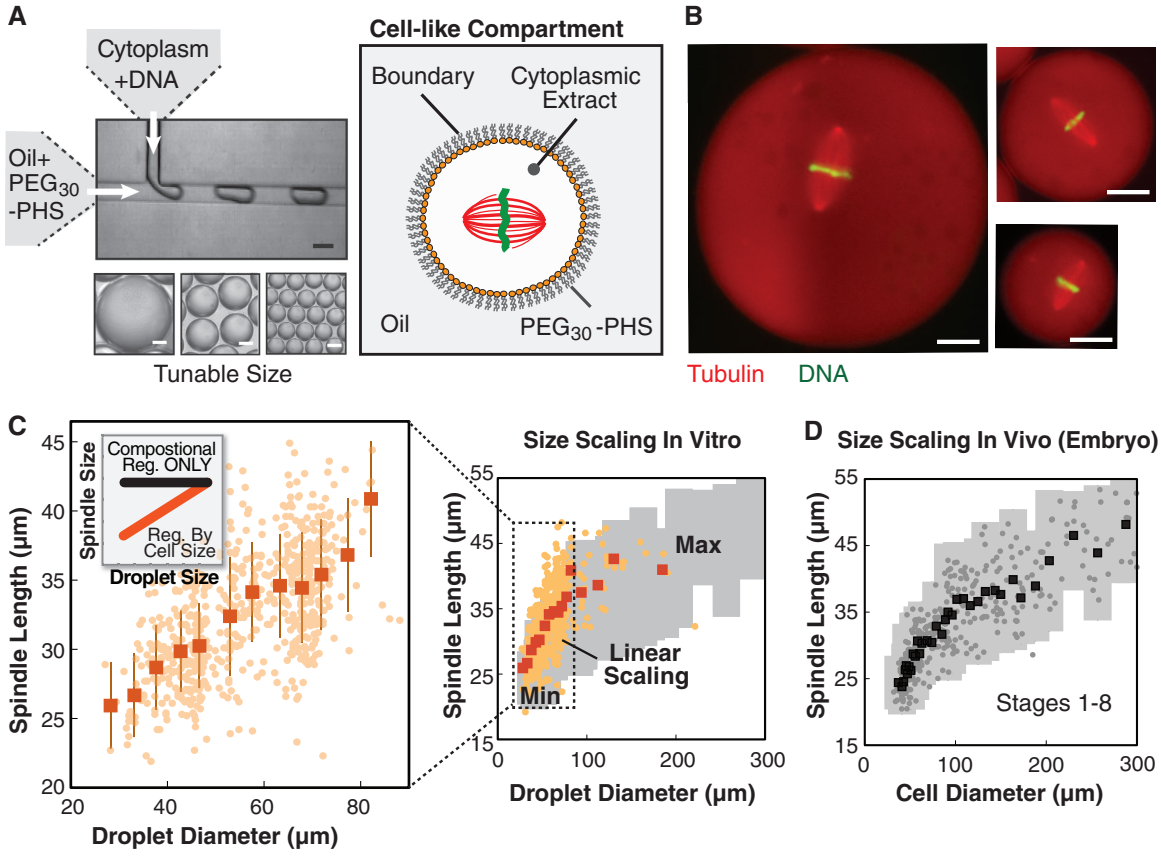

Fig. 1. Spindle length scales with compartment size in vitro and in vivo. (**A**) System for creating cell-like compartments in vitro, including a passivated boundary, cell-free cytoplasm capable of assembling metaphase spindles (*Xenopus* egg or embryo extracts), and tunable compartment size. PHS, polyhydroxystearate. (**B**) Spindles in droplets, compressed to improve image quality, corresponding to spheres 80, 55, and 40 μm in diameter. Uneven shading is due to image stitching. Scale bars indicate 20 μm. (**C**) Spindle length in encapsulated *X. laevis* egg extract scaled with droplet size in vitro. (Left) Linear scaling regime. (Inset) Scaling prediction. Raw data (orange circles) and average spindle length (orange squares) ± SD across 5-μm intervals in droplet diameter are shown. *P* value ($<10^{-60}$) and R^2 (0.34) calculated from linear fit to raw droplet data in 20- to 80-μm diameter range. (Right) Full scaling curve in vitro. For comparison, gray bars indicate two standard deviations from average embryo data in (D). (**D**) Spindle length scaling in vitro mirrored length scaling in the *X. laevis* embryo through stage 8, with similar linear scaling regimes and a plateau where spindle size was uncoupled from compartment size. Raw data from embryos across 5-μm intervals in cell diameter (gray circles) and average spindle length (black squares) ± 2 SD (thick error bars) are shown.

between these two possibilities, we compared spindle size scaling in droplets that were spherical or compressed into a disklike shape (z-height ~ 25 μm) (fig. S4B). Spindle length and assembly efficiency in differently shaped droplets collapsed onto the same curve when plotted against volume but not diameter, suggesting that spindle assembly is dependent on the amount of cytoplasm rather than the position of the compartment boundaries (Fig. 2 and fig. S4C). Although spindles were positioned near the center of cells in the embryo, they were more randomly distributed when formed in droplets (fig. S4D) (*23*). Although the cell boundary plays a crucial role in positioning and could affect spindle size in vivo, we did not observe an effect in droplets. Thus compartment volume, not boundary interactions, dictates spindle size in our system.

To elucidate how spindle size scales with compartment volume, we considered a limiting component mechanism, in which the amount of particular molecules per cell regulates spindle assembly. Although multiple components could become limiting, we focused our attention on tubulin, the subunit of microtubules and the major structural component of the spindle, whose levels have been implicated in regulating spindle size (*24*). Because the cellular tubulin concentration and the number and length of microtubules in the egg extract spindle have been characterized (*25*, *26*), it was possible to determine what fraction of soluble tubulin within a given volume remained in the cytoplasm after spindle assembly. We used this information to create a simplified quantitative model that predicted spindle size on the basis of compartment volume (Fig. 3A and fig. S5). The model assumes an available pool of soluble αβ-tubulin dimers, which is depleted as the spindle assembles, and depends on both cytoplasmic volume and spindle volume. Because tubulin concentration is known to affect microtubule dynamics (*27*, *28*), we hypothesized that this depletion might drive volume-dependent spindle scaling. Combining this idea with measured spindle parameters (*25*, *26*) and the observation that tubulin density in the spindle does not change with spindle size (fig. S6B, inset) (*29*), we derived an analytical model for volume-dependent spindle scaling that agrees quantitatively with our data both in droplets (Fig. 3B and fig. S5C) and in cells during embryogenesis (fig. S5D) (*23*).

A key prediction of this model is that the soluble tubulin concentration after spindle assembly should be lower for smaller cells. We measured the fluorescence intensity of tubulin in the cytoplasm and spindle as a function of cell volume (fig. S6A) and found that cytoplasmic tubulin was significantly depleted in cells smaller than 150 μm in diameter, with up to 60% of the total cellular tubulin incorporated into the spindle in the smallest cells (Fig. 3C and fig. S6B). This result is quantitatively consistent with our model (Fig. 3C) and rules out other models in which the spindle assembles from a constant fraction of cellular material. Although our analysis suggests that tubulin is necessary to maintain spindle size, it is not likely to be sufficient. The addition of tubulin to egg extracts did not alter spindle scaling in droplets (fig. S7), presumably because the levels of other spindle assembly factors were also limiting. In summary, although the model described here is general and can be applied to other molecular components that are enriched in the spindle, its quantitative agreement with measured data suggests that tubulin depletion plays an important role in volume-dependent spindle scaling.

Volume offers a useful mechanism for directly modulating spindle size throughout development. Because cell size varies within an embryo and even within individual stages of development (fig. S8A), scaling mechanisms based only on developmental timing or cytoplasmic composition would not couple spindle size to cell size, potentially leading to spindle positioning errors. We found that spindle length and cell volume correlated across most stages of *X. laevis* early embryogenesis (Fig. 4A) and within individual developmental stages (fig. S8, B and C), in support of volume-dependent scaling in vivo. To demonstrate that cytoplasmic volume regulates spindle size independent of developmental stage, we encapsulated stage 4 (8-cell) and stage 8 (~4000-cell) embryo extracts. In the largest droplets, maximum spindle size was consistent with results in unencapsulated extracts (*30*) and depended on developmental stage (Fig. 4B). Nonetheless, encapsulated mitotic spindles from both extracts exhibited volume-dependent scaling (Fig. 4B), showing that cytoplasmic volume and composition together control spindle size during *X. laevis* embryogenesis.

To determine whether cytoplasmic volume-dependent spindle scaling is conserved in other organisms, we encapsulated egg extracts from a related frog species, *Xenopus tropicalis*, which generate smaller spindles than *X. laevis* extracts, in part because of higher microtubule-severing activity of p60 katanin (*20*, *31*). Like *X. laevis* spindles, *X. tropicalis* spindles scaled with compartment volume, both in vitro (fig. S9, A and B) and in vivo (fig. S10B). Combined with recent data for spindle size in embryos of the mammal *Mus musculus* (*17*), these findings indicate conservation of volume-dependent scaling in vertebrate evolution. Although the upper limits to spindle size vary in embryonic cells among these organisms (fig. S10C), large portions of the scaling curves closely overlapped (fig. S10D).

Taken together, these results suggest that volume-dependent spindle size scaling is conserved across spindle architectures (meiotic and mitotic), developmental stages, and vertebrate species. Previous reports on spindle scaling factors have focused primarily on compositional differences between cells or cytoplasmic extracts. We have identified cell volume as a physicochemical scaling mechanism that regulates spindle size through limiting amounts of cytoplasmic material, acting in concert with other mechanisms that alter activity of microtubule regulatory factors (*26*, *29*–*31*). All together, mechanisms altering

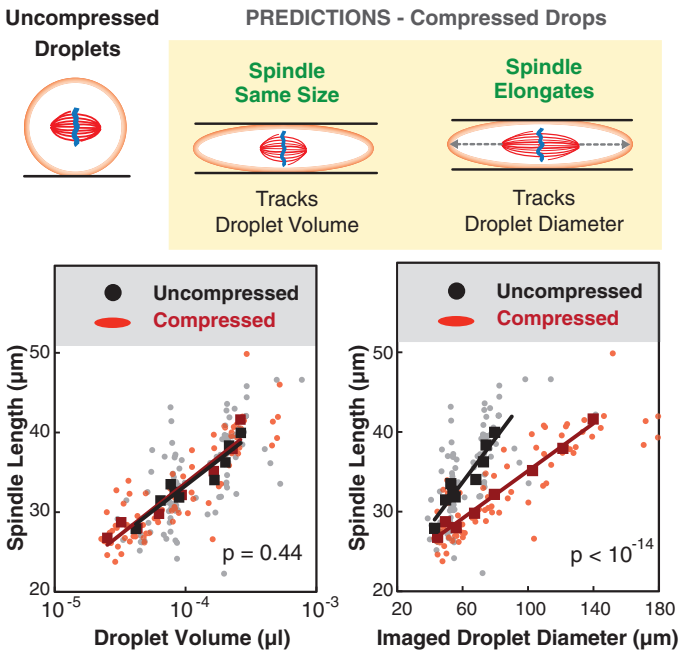

Fig. 2. Cytoplasmic volume sets spindle size in vitro. To distinguish between boundary- and volume-sensing models, we compared spindle length scaling in uncompressed (spherical) and compressed (disklike) droplets (details in fig. S4B). Spindle length scaling in both droplet geometries appeared identical when plotted as a function of droplet volume, supporting a volume-sensing mechanism. Spindle scaling curves did not overlay when plotted as a function of projected (imaged) droplet diameter, ruling out boundary sensing. Raw data points (circles; gray, uncompressed; red, compressed) and spindle length, averaged across 10 droplets (squares; black, uncompressed; red, compressed), are shown. Raw data were fit to a log function in volume plot [black line, R^2 = 0.42 (uncompressed), and red line, R^2 = 0.79 (compressed)] and linear function in diameter plot [black line, R^2 = 0.45 (uncompressed), and red line, R^2 = 0.79 (compressed)]. *P* values indicate statistical differences between *y* intercepts of compressed versus uncompressed regression lines, calculated by using an analysis of covariance.

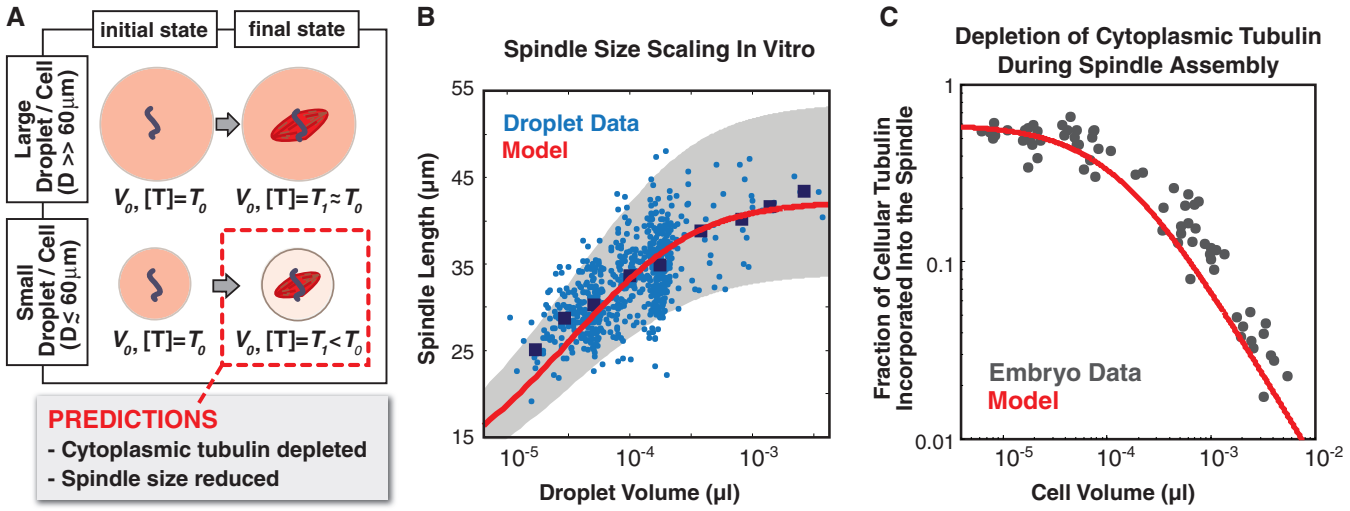

Fig. 3. A limiting-component model for spindle size regulation. (**A**) Schematic of limiting-component model (for more details, see fig. S5A and supplementary text). (**B**) Limiting tubulin model accurately predicted *X. laevis* spindle length from droplet volume in vitro. Raw data from droplets (blue circles) and binned averages (dark blue squares) were compared to the model. Shaded gray regions represent model predictions across a range of parameter values (fig. S5B); the red line shows the prediction for intermediate values. (**C**) Cytoplasmic tubulin became substantially depleted as cell size decreased during *X. laevis* embryogenesis. Comparison of model prediction (red) and experimental data (gray) for the fraction of total cellular tubulin incorporated in the spindle as a function of cell volume. Model used parameter values that gave best agreement in fig. S5, C and D.

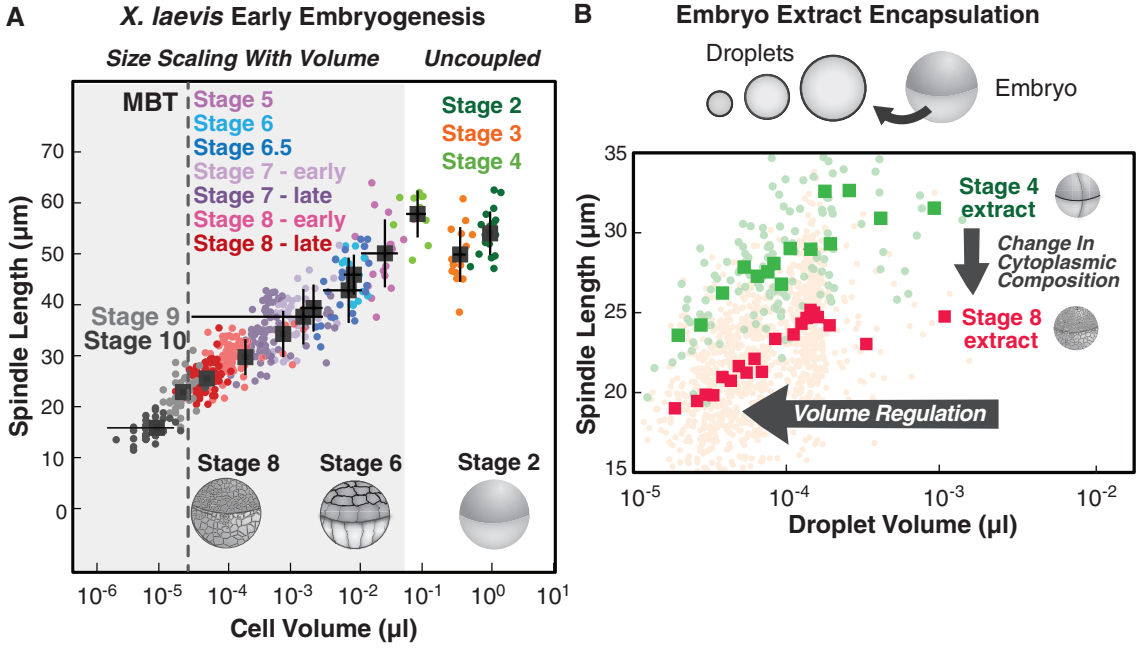

Fig. 4. Cell volume and composition control spindle size during *Xenopus* early embryogenesis. (**A**) Spindle length scaled linearly with cell volume across a broad range of developmental stages during early *X. laevis* embryogenesis (stages 5 to 10). Spindle length had an upper limit and was uncoupled from cell volume in stages 2 to 4. Raw data (colored circles) and stage-averaged cell diameter and spindle length (black squares) ± SD are shown. (**B**) Despite having distinct maximum spindle lengths coupled to developmental stage (stage 4, green; stage 8, red), the length of *X. laevis* embryo extract mitotic spindles scaled with compartment volume in vitro. This result suggested that changes in cytoplasmic volume and composition work in concert to regulate spindle size. Raw data points (light circles) and bin-averaged spindle length (squares), calculated for 5-μm intervals in droplet diameter across the 20- to 80-μm range of droplet diameters (wider intervals were used for averaging in largest droplets because data were sparse), are shown.

the concentration or activity of cytoplasmic scaling factors appear to modulate maximum and minimum spindle size, whereas cytoplasmic volume couples spindle size to cell size (fig. S11). We propose that the amounts of certain molecules known to be important for spindle assembly, including but not limited to tubulin, are responsible for this coupling, which weakens as cell volume increases and the components required for assembly are no longer limiting.

References and Notes

1. R. Kafri *et al.*, *Nature* **494**, 480–483 (2013).
2. J. J. Turner, J. C. Ewald, J. M. Skotheim, *Curr. Biol.* **22**, R350–R359 (2012).
3. A. Tzur, R. Kafri, V. S. LeBleu, G. Lahav, M. W. Kirschner, *Science* **325**, 167–171 (2009).
4. M. Pinot *et al.*, *Curr. Biol.* **19**, 954–960 (2009).
5. M. Pinot *et al.*, *Proc. Natl. Acad. Sci. U.S.A.* **109**, 11705–11710 (2012).
6. L. Laan *et al.*, *Cell* **148**, 502–514 (2012).
7. N. Minc, D. Burgess, F. Chang, *Cell* **144**, 414–426 (2011).
8. O. M. Lancaster *et al.*, *Dev. Cell* **25**, 270–283 (2013).
9. M. Wühr *et al.*, *Curr. Biol.* **18**, 1256–1261 (2008).
10. Y. H. Chan, W. F. Marshall, *Science* **337**, 1186–1189 (2012).

11. S. Dumont, T. J. Mitchison, *Curr. Biol.* **19**, R749–R761 (2009).
12. N. W. Goehring, A. A. Hyman, *Curr. Biol.* **22**, R330–R339 (2012).
13. G. Goshima, J. M. Scholey, *Annu. Rev. Cell Dev. Biol.* **26**, 21–57 (2010).
14. D. L. Levy, R. Heald, *Annu. Rev. Cell Dev. Biol.* **28**, 113–135 (2012).
15. G. Greenan *et al.*, *Curr. Biol.* **20**, 353–358 (2010).
16. Y. Hara, A. Kimura, *Mol. Biol. Cell* **24**, 1411–1419 (2013).
17. A. Courtois, M. Schuh, J. Ellenberg, T. Hiiragi, *J. Cell Biol.* **198**, 357–370 (2012).
18. A. Desai, A. Murray, T. J. Mitchison, C. E. Walczak, *Methods Cell Biol.* **61**, 385–412 (1998).
19. E. Hannak, R. Heald, *Nat. Protoc.* **1**, 2305–2314 (2006).
20. K. S. Brown *et al.*, *J. Cell Biol.* **176**, 765–770 (2007).
21. M. Decker *et al.*, *Curr. Biol.* **21**, 1259–1267 (2011).
22. E. G. Conklin, *J. Exp. Zool.* **12**, 1–98 (1912).
23. A description of the spindle centering analysis and a detailed derivation of the limiting component model can be found in the supplementary materials.
24. R. Lattao, S. Bonaccorsi, M. Gatti, *J. Cell Sci.* **125**, 584–588 (2012).
25. J. Brugués, V. Nuzzo, E. Mazur, D. J. Needleman, *Cell* **149**, 554–564 (2012).
26. R. Loughlin, R. Heald, F. Nédélec, *J. Cell Biol.* **191**, 1239–1249 (2010).
27. L. Brun, B. Rupp, J. J. Ward, F. Nédélec, *Proc. Natl. Acad. Sci. U.S.A.* **106**, 21173–21178 (2009).
28. M. E. Janson, M. E. de Dood, M. Dogterom, *J. Cell Biol.* **161**, 1029–1034 (2003).
29. S. B. Reber *et al.*, *Nat. Cell Biol.* **15**, 1116–1122 (2013).
30. J. D. Wilbur, R. Heald, *eLife* **2**, e00290 (2013).
31. R. Loughlin, J. D. Wilbur, F. J. McNally, F. J. Nédélec, R. Heald, *Cell* **147**, 1397–1407 (2011).

Acknowledgments: This work was supported by fellowships from the Miller Institute for Basic Science Research (M.C.G.), NIH (M.D.V.), and NSF (A.S.). This work was also supported by NIH grants (GM074751, D.A.F.) and (GM098766, R.H.). We thank J. Wilbur, K. Helmke, F. Nedelec, K. Weis, M. Welch, H. Ramage, K. Nyberg, N. Metrakos, the Berkeley BioChIP NSF Research Experience for Undergraduates program, and members of the Heald and Fletcher labs. The authors declare no competing financial interests. Data described can be found in the main figures and supplementary materials.

Supplementary Materials

www.sciencemag.org/content/342/6160/856/suppl/DC1
Materials and Methods
Supplementary Text
Figs. S1 to S11
References (*32*–*39*)

12 July 2013; accepted 15 October 2013
10.1126/science.1243147

ERF115 Controls Root Quiescent Center Cell Division and Stem Cell Replenishment

Jefri Heyman,[1,2] Toon Cools,[1,2] Filip Vandenbussche,[3] Ken S. Heyndrickx,[1,2] Jelle Van Leene,[1,2] Ilse Vercauteren,[1,2] Sandy Vanderauwera,[1,2] Klaas Vandepoele,[1,2] Geert De Jaeger,[1,2] Dominique Van Der Straeten,[3] Lieven De Veylder[1,2]*

The quiescent center (QC) plays an essential role during root development by creating a microenvironment that preserves the stem cell fate of its surrounding cells. Despite being surrounded by highly mitotic active cells, QC cells self-renew at a low proliferation rate. Here, we identified the ERF115 transcription factor as a rate-limiting factor of QC cell division, acting as a transcriptional activator of the phytosulfokine PSK5 peptide hormone. ERF115 marks QC cell division but is restrained through proteolysis by the APC/C^{CCS52A2} ubiquitin ligase, whereas QC proliferation is driven by brassinosteroid-dependent *ERF115* expression. Together, these two antagonistic mechanisms delimit ERF115 activity, which is called upon when surrounding stem cells are damaged, revealing a cell cycle regulatory mechanism accounting for stem cell niche longevity.

Plant root growth and development depend on the continuous generation of new cells by the stem cell niche that is located in the proximal zone of the root meristem. Key to the maintenance of the stem cell niche are a small group of organizing cells, the quiescent center (QC) (*1*–*4*). QC cells divide with a frequency lower by a factor of 3 to 10 than mitotically active root cells (*2*, *5*–*7*). Combined with the suppression of stem cell differentiation, a low QC proliferation rate is fundamental to maintain root structure and meristem function (*7*). Whereas inhibition of stem cell differentiation is controlled through the retinoblastoma pathway (*8*), the molecular components that control the QC cell division rate remain unknown. The *Arabidopsis thaliana* CELL CYCLE SWITCH 52 A2 (CCS52A2) activating subunit of the anaphase-promoting complex/cyclosome (APC/C), a highly conserved E3 ubiquitin ligase that marks cell cycle proteins for destruction, restrains QC cell division (*9*).

[1]Department of Plant Systems Biology, VIB, B-9052 Gent, Belgium. [2]Department of Plant Biotechnology and Bioinformatics, Ghent University, B-9052 Gent, Belgium. [3]Laboratory of Functional Plant Biology, Department of Physiology, Faculty of Sciences, Ghent University, B-9000 Gent, Belgium.

*Corresponding author. E-mail: lieven.deveylder@psb.vib-ugent.be

CCS52A2 copurifying proteins identified through tandem-affinity purification (fig. S1) (*10*) were screened for their ability to promote QC cell proliferation upon ectopic expression. Among these, the ethylene response factor 115 (ERF115) resulted in a QC cell division phenotype that mimicked that of *ccs52a2-1* knockout plants (Fig. 1, A to C). Expression of the WOX5-GFP (green fluorescent protein) marker confirmed that it was the QC cells that divided (fig. S2).

ERF115 (At5g07310) belongs to the ETHYLENE RESPONSE FACTOR family of transcription factors that control the transcription of genes linked to various biological processes related to growth and development. Biochemical data validated that ERF115 is a proteolytic target of APC/C^{CCS52A2}. The proteasome inhibitor MG132 stabilized the chimeric ERF115-GFP reporter in a *CCS52A2*-dependent manner (Fig. 1, D to G, and fig. S3). In contrast, knockout of the paralogous *CCS52A1* gene, which controls the timing of cell cycle exit of the root cells within the cell elongation zone through cyclin destruction (*6*, *11*), did not affect proteolysis of ERF115 (Fig. 1, H and I). ERF115 has two putative destruction (D)–box sequences (amino acids 115 to 118 and 150 to 153) that are recognized by the APC/C (fig. S4A). Inactivation of the proximal D-box stabilized ERF115, whereas its stability was increased by mutation of the second D-box (Fig. 1J and fig. S4B).

In agreement with ERF115 being a proteasome target, within translation reporter lines, ERF115-GFP fluorescence could only be detected upon MG132 treatment, revealing a QC cell–specific accumulation pattern (fig. S5). Correspondingly, *ERF115* promoter activity was observed in the QC cells (Fig. 2A), albeit only in 11.7% of the examined roots (n = 60 root tips). As observed previously (*6*), a modest temperature increase promoted QC cell division (31.0% at 24°C versus 15.0% at 21°C; n = 20 and 29 roots, respectively), coinciding with a temperature-dependent rise in *pERF115:GUS*-positive QC cells (Fig. 2C), of which 32.3%, corresponding to the QC cell division frequency at 24°C, showed signs of a recent cell division, as indicated by the presence of two adjacent blue cells (Fig. 2B). When grown with the cell cycle inhibitory drug hydroxyurea, plants had fewer *pERF115:GUS*-positive QC cells (Fig. 2C). Thus, *ERF115* expression marks dividing QC cells.

Ethylene plays a putative role in QC cell division (*5*) and regulates some members of the *ERF* gene family. However, the frequency of *pERF115:GUS*-positive QC cells did not vary upon treatment with the ethylene precursor 1-aminocyclopropane-1-carboxylic acid (ACC) or ethylene itself, nor upon treatment with the ethylene inhibitor silver nitrate (fig. S6), suggesting that ERF115 is not involved in ethylene perception or signaling. Brassinosteroids also promote QC cell division (*12*). Correspondingly, *ERF115* expression appeared to depend on brassinosteroids, because treatment with brassinolide increased the number of *pERF115:GUS*-positive QC cells (Fig. 2C and fig. S7) and reached up to 86.6% (n = 82 root tips) at 24°C. Because of the link between *ERF115* expression and QC cell division, we investigated whether the brassinosteroid-dependent QC cell proliferation phenotype was ERF115 dependent. QC cells of *erf115*^{KO} lines still divided in response to brassinosteroid treatment, perhaps due to gene redundancy in the 122-member *ERF* gene family. To circumvent this problem, we converted